Tuneable and robust long range surface plasmon resonance for biosensing applications

Régis Méjard [a], Jakub Dostálek [b], Chun-Jen Huang [b], Hans Griesser [a], Benjamin Thierry [a,*]

[a] Ian Wark Research Institute, University of South Australia, Mawson Lakes Campus, Mawson Lakes, South Australia, Australia
[b] AIT – Austrian Institute of Technology, Muthgasse 11, 1190 Vienna, Austria

ABSTRACT

A multilayered biosensing architecture based on long range surface plasmons (LRSPs) is reported. LRSPs originate from the coupling of surface plasmons on the opposite sides of a thin metal film embedded in a symmetrical refractive index environment. With respect to regular SPs, LRSPs are characterized by extended electromagnetic field profiles and lower losses, making them of high interest in biosensing, especially for large biological entities. LRSPs-supporting layer structures are typically prepared by using fluoropolymers with refractive indices close to that of water. Unfortunately, fluoropolymers have low surface energies which can translate into poor adhesion to substrates and sub-optimal properties of coatings with surface plasmon resonance-active metal layers such as gold. In this work, a multilayered fluoropolymer structure with tuneable average refractive index is described and used to adjust the penetration depth of LRSP from the sensor surface. The proposed methodology also provides a simple solution to increase the adhesion of LRSP-supporting structures to glass substrates. Towards taking full advantage of long range surface plasmon resonance sensors, a novel approach based on the plasma-polymerization of allylamine is also described to improve the quality of gold layers on fluoropolymers such as Teflon AF. Through these advancements, long range surface plasmon resonance sensors were fabricated with figures of merit as high as 466 RIU^{-1}. The remarkable performance of these sensors combined with their high stability is expected to foster applications of LRSPR in biosensing.

© 2013 Elsevier B.V. All rights reserved.

1. Introduction

Surface plasmon resonance (SPR) is a phenomenon associated with the coupling of light and collective oscillations of electrons at a metal-dielectric interface [1]. These oscillations are referred to as surface plasmon (SP) waves and their confined electromagnetic fields make them excellently suited to the characterization of binding interactions of biomolecules on metallic surfaces. In biosensing applications, the liquid sample to be analyzed is brought in contact to the metallic sensor surface that carries the biomolecular recognition elements. The specific binding of the target molecules to the biomolecular recognition elements is probed by resonantly excited SPs. Under such conditions, binding events result in local refractive index variations that are directly observed from changes in the SPR reflectivity signal [2]. In addition, SP provides a basis for powerful amplification strategies in other important optical bioan-alytical methods including surface-enhanced Raman spectroscopy, IR spectroscopy, and fluorescence spectroscopy [3–5]. In analytical technologies exploiting plasmonic structures, the characteristics of SPs should be tailored in order to maximize the sensitivity. For example, decreasing losses of SPs lead to narrower resonance profiles and higher field-intensity enhancements which directly translate into improved refractometric sensor accuracy [6]. In addition, tuning the penetration depth in the sensing medium of the SP fields allows for optimum overlap with the employed biointerface and can suppress undesired effects interfering with SPR measurements [7]. This can be achieved using long range surface plasmon (LRSP) resonance sensors.

LRSP waves originate from the coupling of surface plasmons on the opposite surfaces of a thin metallic film embedded between two dielectrics with similar refractive indices. LRSP waves were first reported in the early 80's by Sarid [8]. LRSP waves exhibit extended electromagnetic field profiles and lower losses compared to conventional SPs. These excellent optical properties have been taken advantage of in numerous optical technologies [9–11]. While conventional SPR has been used successfully to detect large biological analytes such as bacteria [12–14] and living cells [15–18], only small portions of the target cells/bacteria are within the

evanescent waves. On the other hand, the characteristic features of long range surface plasmon resonance (LRSPR) make it particularly attractive for the analysis of such living organisms [19,20]. In addition, LRSPR is compatible with the probing of advanced biointerface architectures with characteristic thicknesses of around one micrometer that can accommodate large amounts of target analytes and thus generate strong signals [21,22].

Biosensors utilizing LRSPs typically rely on layer architectures comprising a thin noble metal film deposited on a dielectric layer (buffer layer) with a refractive index close to that of water. Besides oxide layers such as magnesium fluoride (MgF_2) [9] or aluminum fluoride (AlF_3) [23], fluoropolymers exhibiting refractive indices close to 1.33 are preferably used owing to the existence of simple deposition methodologies and possible structuring by nano-imprint lithography (NIL) [24]. The majority of LRSPR studies have indeed relied on either a polymer made by cyclopolymerization of the perfluorinated diene, perfluoro-(4-vinyloxy-1-butene) (Cytop from ASAHI Inc., Japan) or an amorphous copolymer of polytetrafluoroethylene (PTFE) with 2,2-bis(trifluoromethyl)-4,5-difluoro-1, 3-dioxole (Teflon AF from DuPont, USA). Although Teflon AF is, from an optical standpoint, advantageous over Cytop towards the design of LRSPR sensors, the use of Teflon AF presents a number of challenges associated with the low surface energies of such fluoropolymers. The first challenge is an intrinsic poor adhesion on glass substrates, which makes sensors prone to delamination and consequently unstable over time. The adhesion strength of Teflon AF to glass surfaces can be increased using silane linker layers [6,19] but the latter modification requires rather complex protocols. In addition, in our experience, the resulting improvement is only transient and stability remains an issue for long term studies or middle to long-term storage. The second challenge associated with Teflon AF is the poor quality of the gold layers deposited on Teflon AF, which drastically impacts on the performances of LRSPR sensors. Despite their merits in conventional SPR, chromium or titanium gold-adhesion layers [20,25] dramatically increase losses of LRSPs (as they propagate along both sides of the gold film) and thus they are detrimental for LRSPR biosensing applications.

This study focuses on solving these two key issues associated to the use of Teflon AF-based LRSPR biosensors. To this end, a new multilayered architecture that provides strong adhesion of Teflon AF on glass was first developed. Importantly, this multilayered architecture enables tuning the profile of field of LRSPs through adjusting the (average) refractive index of the fluoropolymer buffer layer. Next, we investigated new approaches for improving the quality of thin gold films on fluoropolymer surfaces including the use of a solvent-free plasma-polymerized allylamine (PPAA) adhesion layer. Ultimately, this work aimed at the development of more robust LRSPR sensors towards fully harnessing the excellent potential of LRSPs in analytical technologies, especially for the detection and observation of interactions of molecular and biological species.

2. Materials and method

2.1. Materials

Ethanol, chlorotrimethylsilane (CTMS), perfluorooctyltrichlorosilane (PFOCS), hexadecane and chloroform were purchased from Sigma–Aldrich (USA). Teflon AF 1600 was obtained from DuPont (USA) and dissolved to the grade 10% (w/v) in FC-40 from 3 M (USA). Cytop (CTL-809 M, 9 wt%) and its solvent perfluorotrialkylamine (CT-SOLV 180) were purchased from Asahi Glass (Japan). Allylamine 98% was purchased from Sigma–Aldrich. Hellmanex II and LaSFN9 glass substrates were obtained from Hellma Optik (Germany). Poly(dimethylsiloxane) (PDMS) was acquired from Dow Corning (Singapore).

2.2. Preparation and characterization of samples

LRSPR sensors were prepared on LaSFN9 glass slides. The slides were sonicated in Hellmanex for 20 min followed by 20 min of sonication in milliQ water and final copious rinsing with milliQ water. Glass slides were then dried at 150 °C on a hot plate for 10 min. Silane CTMS and PFOCS adhesion layers were deposited from vapor and liquid phases, respectively using standard protocols. Hexadecane and chloroform were used as solvents (4:1) for liquid-phase silanization of PFOCS (0.1 mM) which was carried out under nitrogen atmosphere. The clean glass substrates were immersed for 15 minutes in the PFOCS solution and then rinsed with ethanol and dried in a stream of nitrogen gas.

Cytop layers were prepared by spincoating followed by drying of the deposited fluoropolymer layer at 60 °C for 5 min then 150 °C for 30 min. Under the chosen experimental conditions, the thickness of the Cytop layers was approximately 30 nm (1:8 dilution with perfluorotrialkylamine, rotation speed 2500 revolutions per minute [rpm] for 30 s, acceleration 500 rpm/s), 20 nm (1:7 dilution, 2600 rpm for 30 s, 500 rpm/s) and 750 nm (undiluted, 1800 rpm for 50 s, 100 rpm/s). Teflon AF layers were prepared by spincoating a 10% Teflon AF solution using a two-step procedure (spinning at 1500 rpm for 10 s with acceleration of 200 rpm/s followed by spinning at 3700 rpm for 50 s with acceleration of 200 rpm/s). The thicknesses of Teflon AF layers were 750 nm and 720 nm for spinning at 3650 and 3700 rpm, respectively.

Plasma polymerization of the allylamine adhesion layers was carried out based on previously reported work [26]. The flow of monomer was set to 10 sccm and the polymerization was carried out at 10 W. A ~3 nm/min deposition rate was determined using a Nanoscope IIIa (Veeco, USA) atomic force microscope (AFM). Gold depositions were performed using a K575X7 sputter coater from Quorom Technologies (UK) with nitrogen pressure set to approximately 10^{-3} mBar. Layer thicknesses were determined by using a NT9100 optical profilometer from Veeco (USA). Atomic Force Microscopy was used to determine the morphologies of the surfaces. The root mean square (rms) roughness was determined from 5 μm × 5 μm scans using the manufacturer software.

2.3. Optical setup for SPR measurements

SPR measurements were conducted using an optical setup based on the attenuated total reflection (ATR) method in the Kretschmann configuration that was developed at the Max Planck Institute for Polymer Research in Mainz (Germany). As shown in Fig. 1, a light beam at a wavelength of $\lambda = 633$ nm (HeNe laser, CVI Melles Griot, USA) passes through two polarizers (Bernhard Halle Nachfl. GmbH, Germany) and a chopper (PerkinElmer Instruments, USA) before being coupled to a LASFN9 glass prism. The intensity of the laser beam reflected from the prism base is
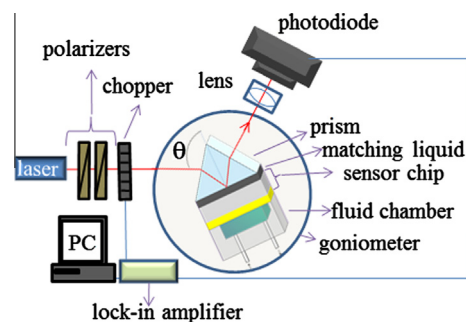

Fig. 1. Optical setup for the excitation and angular interrogation of LRSPs utilizing attenuated total internal reflection method.

detected by a photodiode detector and a lock-in amplifier (Signal Recovery, USA). The SPR sensor chip is optically matched to the prism base using a refractive index matching oil (Cargille, USA) and a custom made PDMS flow-cell chamber sealed against its surface. The refractive index of the aqueous samples, n_s, used in refractometric measurements is adjusted by dissolving NaCl in water and measured by an Abbe refractometer (Atago, Japan). The angle of incidence, θ, of the laser beam is controlled by a motorized rotation stage (Hans Huber AG, Germany) and the whole system is controlled by the software WasPlas developed at the Max Planck Institute of Polymer Research (Germany).

2.4. Fitting of the reflectivity spectra

Measured reflectivity spectra, $R(\theta)$, were analyzed by fitting a transfer matrix-based model implemented in the Winspall program (Max Planck Institute for Polymer Research, Germany). From the fitting, the thicknesses and the refractive indices, n_m, of the prepared gold layers were determined. Thicknesses of the fluoropolymer layers were fixed in the fitting studies at values determined using profilometry. The refractive indices of Cytop ($n_b = 1.3368$) and Teflon AF ($n_b = 1.3065$), at the wavelength of $\lambda = 633$ nm, were obtained from ellipsometry measurements performed using the Nano-film EP3-SE Imaging Ellipsometer (Accurion GmbH, Germany). The N-LaSF9 prism refractive index ($n_p = 1.84485$) and water refractive index ($n_s = 1.33141$) were obtained from previous measurements. The refractive index of the 4.5 nm-thick plasma-polymerized allylamine film was assumed to be 1.42 [27]. The profiles of the magnetic field intensities were modeled by using the Winspall program for the resonant angles of incidence θ_{res} which correspond to the minimum of the reflectivity dips associated to the coupling to LRSPs. The penetration depths of the LRSP were calculated as $L_p = \lambda/2\pi\sqrt{n_p^2 \sin^2(\theta_{res}) - n_s^2}$. The figures of merit (FOM) were calculated from the angular shifts of the resonance, $\delta\theta_{res}$, due to a refractive index change of a sample on the sensor surface, δn_s, that was divided by the full width at half maximum (FWHM) of the resonance dip, $\Delta\theta_{FWHM}$.

3. Results and discussion

3.1. Concept of tuneable LRSPs layer architecture

In order to excite LRSPs propagating along a thin gold film, a symmetrical refractive index configuration is required to enable SPs propagating on the opposite surfaces to be phase-matched. However, layer structures with a small refractive index asymmetry can still support LRSPs. We hypothesized that this effect can be exploited to tune the penetration depth of LRSPs into the water medium, L_p, based on the structure shown in Fig. 2. It relies on a multilayered buffer structure that comprises two fluoropolymer layers with refractive indices slightly above (Cytop fluoropolymer) and slightly below (Teflon AF) that of water. As seen in simulations presented in Fig. 3, the coupling to LRSPs in the ATR-based configuration (see Fig. 1) is manifested as a very narrow dip in the reflectivity spectrum. For a Teflon AF buffer layer with a thickness of $d_b = 750$ nm and 20 nm thick gold film, the resonance occurs at $\theta_{res} = 47.50°$. The respective profile of the magnetic intensity in Fig. 3 shows that the field of LRSPs overlaps more strongly with the water medium than with the fluoropolymer layer and exhibits a penetration depth of $L_p = 1037$ nm. For an identical structure with a Cytop buffer layer, the resonance occurs at a higher angle of incidence $\theta_{res} = 48.55°$. Therefore, the penetration depth into water is significantly smaller, $L_p = 484$ nm, and the LRSP field is more confined in the fluoropolymer films than in water medium.
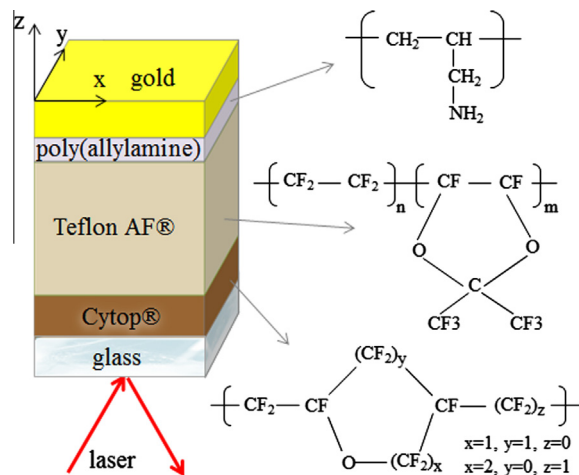

Fig. 2. Schematic of the multilayered structure supporting LRSP proposed in this work. A stack of fluoropolymers constitutes the buffer layer and a plasma-polymerized allylamine thin coating is used to increase the quality of the gold layer. The arrows represent the penetration depth.
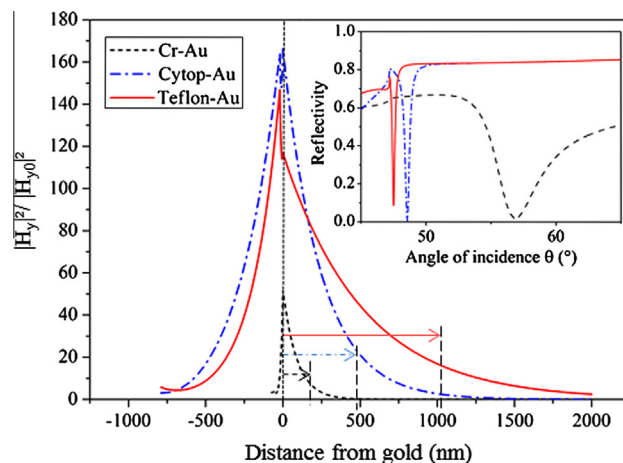

Fig. 3. Comparison of the simulated LRSPs magnetic field intensity profiles at the resonance coupling (20 nm thick gold film) for Cytop (— · — ·) and Teflon AF (——) buffer layers. The data are compared to those of regular SPR (– – –). A refractive index of gold of $n_m = 0.282 + 3.12i$ ($\varepsilon_m = -9.65 + 1.76i$) was assumed for LRSPR structures and $n_m = 0.186 + 3.498i$ ($\varepsilon_m = -9.65 + 1.3i$) for the SPR structure.

The data presented in Fig. 3 illustrate that small variations of the average refractive index of the multilayered buffer structure between $n_b = 1.3065$ and 1.3368 allows tuning the LRSP penetration in a wide range ($L_p = 484$–1037 nm). More generally, plotting L_p as a function of n_b reveals the dependence of these parameters as shown in Fig. 4a. This phenomenon is further exploited for tuning the L_p within the range [484–1037] by using a buffer structure that is composed of a stack of Cytop and Teflon AF layers with a total thickness of $d_b = 750$ nm, see Fig. 2. Fig. 4b shows that by changing the thickness of the Cytop layer d_{b-Cyt} the average refractive index of the (composite) buffer layer is altered and thus L_p can be tuned. The total thickness of the buffer structure was kept constant and the thickness of the Teflon AF layer was adjusted to $d_{b-Tef} = d_b - d_{b-Cyt}$. In addition, the presence of a gold-adhesion layer (e.g. plasma-polymerized allylamine) was omitted in these simulations for simplicity.

3.2. Stability of Teflon AF layers on glass

In order to develop robust LRSPR sensors, good adhesion of the fluoropolymer buffer layers on glass is critical. The latter is
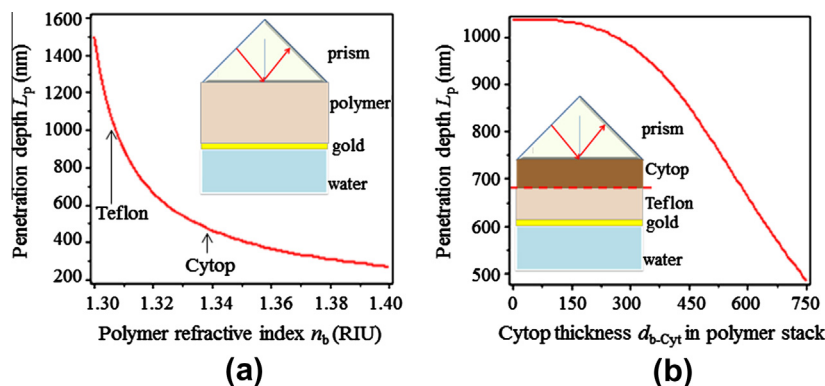
Fig. 4. Simulations of LRSP penetration depth L_p (20 nm thick gold film) and (a) a buffer layer with a refractive index between n_b = 1.3 and 1.5 and (b) fluoropolymer buffer multilayer composed of a stack of Cytop and Teflon AF films. The total thickness is kept at d_b = 750 nm and the thickness of d_{b-Cyt} varies between 0 and 750 nm (the thickness of Teflon AF was changed as $d_{b-Tef} = d_b - d_{b-Cyt}$).

especially a challenge for Teflon AF which typically shows very poor adhesion and is prone to delamination. Silane linker layers are typically used and we compared here two common silanization agents, CTMS and PFOCS. Building on the tuneable LSPR structure described before, these silane adhesion layers were compared to that of the Teflon AF-based multilayered structures where Cytop was used to promote the adhesion of Teflon AF to the glass substrate.

The stability in solution and shelf-life was inferred from changes in the measured LRSPR spectra. For the CTMS linker layer, the degradation of the LRSPR chip in contact with water occurred after only a few minutes. On the contrary, PFOCS adhesion layers provided significantly enhanced stability of the sensor and no change in the LRSPR spectrum was observed for the first 90 min of contact with water, in good agreement with previous LRSPR study [20]. Despite this notable improvement, the shelf-life of these sensors was poor as after 10 days of storing in air the Teflon AF layer rapidly delaminated when incubated with water. The insufficient shelf-life of the layer structure relying on CTMS and PFOCS linker layers and the complex preparation procedure motivated the development of an alternative approach.

Despite its inferior optical properties in comparison to Teflon AF in regards to the performances of LRSPR sensors, Cytop has a good adhesion to glass. It was therefore hypothesized that, in addition to providing a means to control the average refractive index of the buffer film as described above, Cytop could also be used as an adhesion layer for Teflon AF. For a layer structure comprising Cytop layer with a thickness of d_{b-Cyt} = 30 nm between the Teflon AF and the glass substrate, LRSPR spectra did not show measurable changes after the sensor was stored for more than 6 months in air at room temperature. Importantly, the thickness of Cytop adhesion layer d_{b-Cyt} could be increased without any detectable change in the stability of the structure.

3.3. Adhesion and morphology of gold layers on Teflon AF

Teflon AF is a material with very low surface energy and consequently thin gold coatings on Teflon AF are typically of poor quality. Deposition of gold films with thicknesses below approximately 25 nm by either sputtering or thermal evaporation results in island morphology, and in turn decreased conductivity and deteriorated optical properties [28]. In conventional SPR sensors, a thin metal adhesion-promoting layer such as chromium is typically used to improve the adhesion of gold to glass. However, the losses of LRSPs modes are dramatically increased due to the strong Cr absorption as these modes are guided along both interfaces of the thin gold film. Therefore, the use of transparent organic adhesion layers to

improve the quality of thin gold layers on Teflon AF was investigated in this work and compared to standard adhesion-promoting approach based on Cr layers.

First, the use of a thin (~20 nm) Cytop layer spin-coated on top of Teflon AF was tested. Cytop exhibits larger surface energy and it was reported to enable the deposition of gold films with good adhesion strength and low roughness [29]. In agreement with a previous study [6], a thin gold film (d_m = 20 nm) sputtered on a thick Cytop layer typically exhibited a rms roughness of about 1 nm (Fig. 4a). On the other hand, gold layer deposited on Teflon AF resulted in a significantly rougher surface (~2.5 nm, Fig. 4b). This difference was not due to the roughness of the underlying polymer layers as they were similar (rms values of ~0.7 nm for Cytop and ~0.6 nm for Teflon AF). It was however observed that the spincoating of a 20-nm thick Cytop film on Teflon AF was accompanied with a dramatic increase of the roughness which varied between 2.3 nm and 18 nm. This effect was attributed to the ability of methyl nonafluorobutyl ethyl (the Cytop solvent) to partially dissolve Teflon AF leading to the occurrence of bulges and holes. When thicker Cytop films (>100 nm) were spin-coated on the Teflon AF, this effect was not observed. However, for such thicknesses, the range of penetration depths, L_p, over which the LRSPR layer architecture can be tuned, would be strongly limited and L_p > 670 - nm could not be reached. This approach was thus abandoned.

Next, we investigated the gas-phase deposition of thin (d_{PPAA} ≈ 4.5 nm) plasma-polymerized adhesion layers. Plasma polymerization processes enable the deposition of conformal coatings with controllable thicknesses and good adhesion onto polymeric substrates, including Teflon [30,31]. Building on previous work [26] and based on the hypothesis that amine-rich plasma polymers would be compatible with the deposition of gold layers of good quality, allylamine (AA) monomer was selected. AFM revealed that no significant morphological changes occurred after the plasma polymerization of the allylamine layer (rms ~0.4 nm) as well as after the deposition of gold (rms ~0.5 nm, Fig. 5c). In addition, an excellent stability was observed and no changes in the properties of the LRSPR sensors were observed after more than 6 months of storage at room temperature.

3.4. Optical properties of gold film supporting LRSPs

Next the detailed optical properties of gold layers deposited onto the plasma-polymerized adhesion layers prepared as described before were determined and compared to those obtained for gold on standard Cr layers (~2 nm). 20 nm thin gold films were deposited on 720 nm thick Teflon AF surface with and without the gold adhesion-promoting layers. The properties of the gold layers
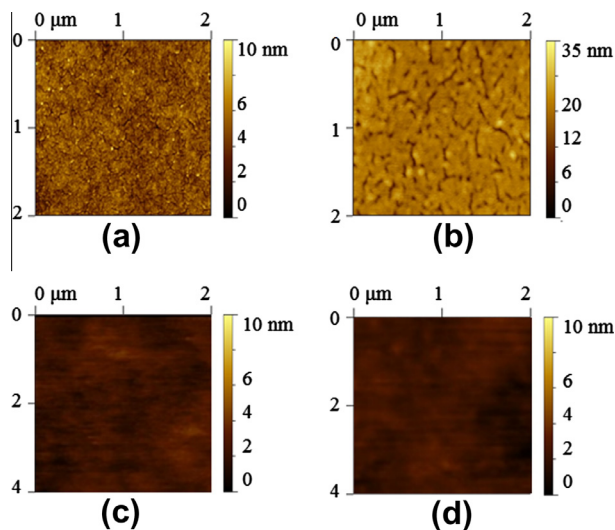
Fig. 5. AFM characterization of 20 nm thick gold layers deposited on the top of (a) Cytop, (b) Teflon AF, (c) Teflon AF coated with 4.5 nm of plasma-polymerized allylamine and d) Teflon AF coated with 1.5 nm of Cr. Note the different z-scales.

were characterized by measuring the angular reflectivity spectrum, $R(\theta)$, in water. The reflectivity dips associated to the resonant excitation of LRSPs were fitted in order to determine the (effective) refractive indices of the gold layers, n_m, (Fig. 6). The complex refractive index n_m relates to the permittivity of the gold film as $n_m = \sqrt{\varepsilon_m}$. The negative real part, ε_m', affects mainly the angular position of the LRSP dip minimum, θ_{res}, and the imaginary part, ε_m'', is strongly related to the losses and width of the resonant dip.

Fig. 6a compares the reflectivity spectra for the tested configurations. One can see that for the stack of fluoropolymer layers without a gold adhesion promoting layer (i.e. gold directly deposited on Teflon AF), the LRSP resonance dip exhibits a minimum at the angle $\theta_{res} = 47.8°$ and a broad width of $\Delta\theta_{FWHM} = 0.67°$. When using PPAA layers, the resonance occurs at a lower angle $\theta_{res} = 47.36°$ and the dip becomes significantly narrower $\Delta\theta_{FWHM} = 0.10°$. When using a standard 2 nm Cr adhesion-promoting layer, the resonance shifted to higher angle $\theta_{res} = 48.55°$ and a higher width of the resonance $\Delta\theta_{FWHM} = 0.44°$ was measured.

The fitting of measured spectra (see respective lines in Fig. 6a) enabled the determination of the gold layer permittivity ε_m for

the different adhesion layers as shown in Fig. 6b. The 20 nm of gold directly deposited on Teflon AF yielded $\varepsilon_m' = -6.00 \pm 1.15$ and $\varepsilon_m'' = 2.75 \pm 0.12$ (error represents the standard deviation). When using the PPAA adhesion layers, higher magnitudes of the permittivity real part $\varepsilon_m' = -10.77 \pm 1.38$ and lower imaginary part $\varepsilon_m'' = 1.87 \pm 0.40$ were observed. These values were close to those obtained for 20 nm of gold deposited on Cytop and therefore in good agreement with the theoretical predictions of Fig. 3. Furthermore, it is noteworthy that these values are close to those measured on regular SPR structures with 50-nm thick gold films and are also in good agreement with values determined by other groups for compact smooth gold layers [6,32]. The fitting of LRSP-supporting structures that comprise Cr layers was not possible indicating that the model used was not valid. This is attributed to the fact that Cr can readily diffuse into the gold layer which is not taken into account in the transfer matrix-based simulations. Hence, the obtained values of gold on top of Cytop–Teflon–Cr structure were not used in the following. Fig.6b illustrates the relation between the gold permittivity and the roughness of the gold surface. This data indicates that increasing roughness is accompanied with a smaller magnitude of the real part of permittivity, ε_m', and with an increase in its imaginary part, ε_m''). From the AFM measurements and the corresponding SPR spectra, a clear correlation between the roughness of the LRSP-gold supporting layer and the spectrum shapes of the sensors was visible. Very smooth surfaces yielded permittivity values close to that of regular SPR structures. This finding indicates that the threshold value of c.a. 25 nm in the gold thickness can be pushed lower and still obtain an optically similar quality of gold [6]. In the case of rough gold surfaces, the permittivity of the gold layer is impacted by a high damping (inversely proportional to the relaxation time), which, in turn yields broader spectra. Additionally, the plasma frequency of the rough gold layers is decreased which leads the resonance conditions to be shifted to the higher angles, thereby reducing the penetration depth, L_p, as per the equation: $L_p = \lambda/2\pi \sqrt{n_p^2 \sin^2(\theta_{res}) - n_s^2}$ [data not shown]. Increased roughnesses will therefore increase the losses of the LRSP-supporting structure and require more confined electromagnetic fields. This is confirmed by the discrepancy with the typical permittivity values of gold from the literature. These considerations are only valid in the case of a transparent material with negligible optical thickness with respect to the bulk of fluoropolymer. For instance, chromium is a very absorbent material and in spite of the very smooth gold surfaces obtained on chromium layers, the corresponding LRSPR spectra is not optimal due to the
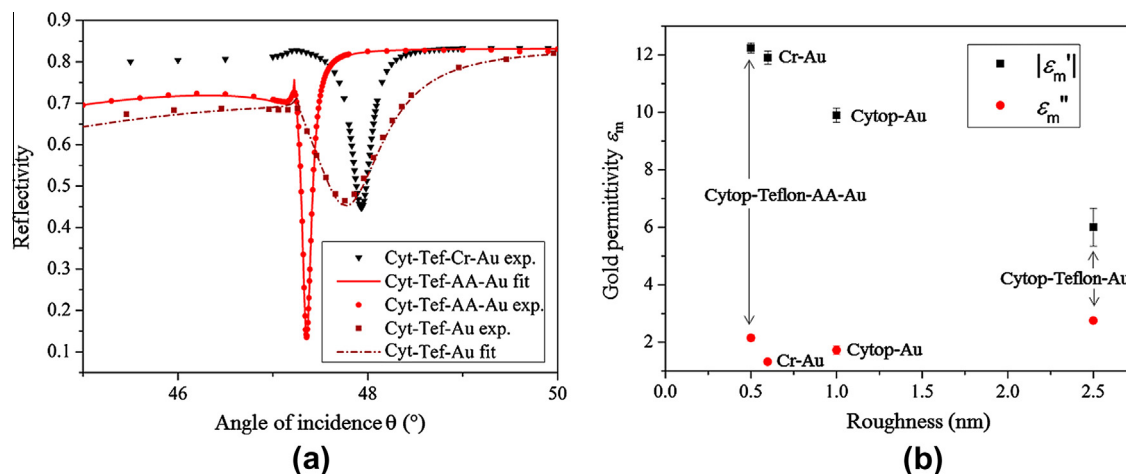
Fig. 6. (a) Comparison of the LRSPR reflectivity spectra for a 20-nm gold film on top of Teflon AF surface (▼), Teflon AF with a 1.5-nm thick chromium layer (■ and —•—•) and Teflon AF with 4.5 nm thick allylamine layer (● and ———). Experimental data are represented as symbols and lines show the fitted curves. (b) Determined permittivity constants as a function of the rms on different surfaces are compared to that of regular SPR sensors.
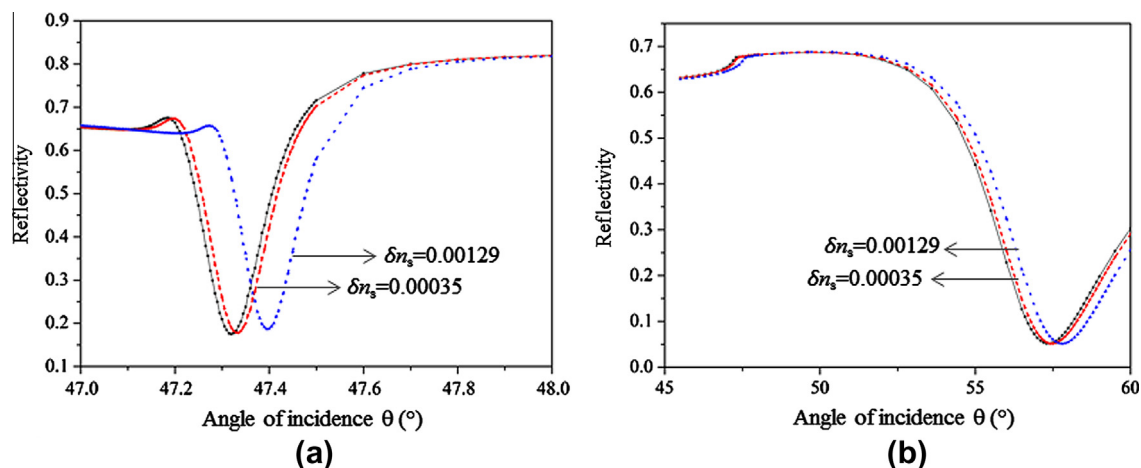
Fig. 7. LRSPR (a) and SPR (b) reflectivity spectra measured for samples with refractive indices of n_s = 1.331415 (– – –), 1.331580 (___ __ __), and 1.332570 RIU (• • • • •). The LRSP-supporting multilayer was constituted of 30 nm Cytop, 720 nm Teflon AF, 4.5 nm of plasma-polymerized allylamine and 20 nm of gold. The $\Delta\theta_{FWHM}$, were respectively 0.10° for LRSPR and 4.8° for regular SPR.

high amount of intrinsic losses induced by the chromium layer into the structure.

These results confirmed that thin PPAA adhesion layers provide excellent performances in terms of coupling efficiency to LRSPs and minimal FWHM width of the resonance. The latter originates in the fact that compact, smooth, thin gold films can be deposited, which do not show the typical island morphology observed on Teflon AF.

3.5. Performance characteristics for LRSP

A refractometric experiment was carried out in order to demonstrate the excellent performance of the developed LRSPR architecture in SPR sensing. In this experiment aqueous solutions with refractive indices of 1.331415, 1.331580, and 1.332570 were injected inside the flow cell and the LRSPR angular reflectivity spectra were recorded. As seen in Fig. 7, the refractive index changes resulted in significant shifts of the LRSP dips. From these data the figure of merit was determined for LRSP-supporting structure with Teflon AF and PPAA. A figure of merit of FOM = 466 RIU^{-1} was determined, significantly better than other structures relying on the excitation of LRSPs on the layer system Cytop buffer layer (FOM = 104 RIU^{-1} [6]) and regular surface plasmon resonance (FOM = 24.3 RIU^{-1}) for gold SPR-active metal (wavelength of λ = 633 nm). To the best of our knowledge, the developed layer architecture provides the highest figure of merit compared to previously reported SPR-based sensing platforms.

3.6. Tolerance and practical aspects of implementation of Teflon AF-based LRSPR

The reproducibility of the allylamine plasma polymerization was found to be good when using low-deposition rates (~0.5 Å/s). Under such conditions, typical batch to batch variations revealed only negligible effects on the LRSPR characteristic features (less than 1% changes in the coupling efficiency and penetration depth). On the other hand, the control of the gold deposition is crucial to achieve high reproducibility LRSPR measurement. Typical errors of ±2 nm in gold layer thicknesses result in large changes in LRSPR spectra and key performance characteristics. For instance, the differences between 18 nm and 22 nm thick gold layers (while keeping all other parameters fixed) leads to changes in the penetration depth of 41% and the coupling efficiency of 23%. Thus, it appears that the main limitation of LRSPR sensors fabrication processes is the necessity to control very accurately the gold

deposition. It is noteworthy that thinner layers of gold could be used to further decrease the losses in LRSP structures. Such thinner layers would result in narrower resonance and higher FOM and to an increase in the penetration depth. However, this would require even more stringent control over gold deposition processes.

4. Conclusions

We report here, on a new fluoropolymer-based multilayered structure which provides excellent resonant excitation of long range surface plasmons propagating along a thin gold film. The multilayered structure allows for straightforward tuning of the profile of the sensing field. The latter is expected to be of high interest for probing of large biological analytes with dimensions greater than the conventional penetration depth of SPs such as bacteria and cells. The quality of the gold layer on the fluoropolymer surface was greatly improved by the deposition of a thin adhesion-promoting plasma-polymerized allylamine layer. This solvent-free layer allowed for the deposition of a thin gold layer of high quality and with high stability. These advancements translated into improved sensitivity in refractometric measurements which was quantified by measuring the figure of merit. In a typical configuration, the FOM was 466 RIU^{-1} which is about 20-times better than that obtained for regular SPR and according to our knowledge the highest reported for SPR-based sensors relying on gold and operated at the wavelength of λ = 633 nm.

References

[1] H. Raether, Surface Plasmons on Smooth and Rough Surfaces and on Gratings, Springer Verlag, Berlin, 1988.
[2] J. Homola, Chemical Reviews 108 (2008) 462–493.
[3] J. Dostalek, W. Knoll, Biointerphases 3 (2008) 12–22.
[4] S. Lal, N.K. Grady, J. Kundu, C.S. Levin, J.B. Lassiter, N.J. Halas, Chem. Soc. Rev. 37 (2008) 898–911.

[5] B. Sharma, R.R. Frontiera, A.-I. Henry, E. Ringe, R.P. Van Duyne, Mater. Today 15 (2012) 16–25.
[6] J. Dostálek, A. Kasry, W. Knoll, Plasmonics 2 (2007) 97–106.
[7] R. Slavik, J. Homola, H. Vaisocherova, Measur. Sci. Technol. 17 (2006) 932–938.
[8] D. Sarid, Phys. Rev. Lett. 47 (1981) 1927.
[9] G.G. Nenninger, P. Tobiška, J. Homola, S.S. Yee, Sens. Actuators B: Chem. 74 (2001) 145–151.
[10] A.W. Wark, H.J. Lee, R.M. Corn, Anal. Chem. 77 (2005) 3904–3907.
[11] P. Berini, Adv. Opt. Photon. 1 (2009) 484–588.
[12] A.D. Taylor, J. Ladd, Q. Yu, S. Chen, J. Homola, S. Jiang, Biosens. Bioelectron. 22 (2006) 752–758.
[13] J.W. Waswa, C. Debroy, J. Irudayaraj, J. Food Process Eng. 29 (2006) 373–385.
[14] F.C. Dudak, I.H. Boyaci, Biotechnol. J. 4 (2009) 1003–1011.
[15] K.F. Giebel, C. Bechinger, S. Herminghaus, M. Riedel, P. Leiderer, U. Weiland, M. Bastmeyer, Biophys. J. 76 (1999) 509–516.
[16] M. Hide, T. Tsutsui, H. Sato, T. Nishimura, K. Morimoto, S. Yamamoto, K. Yoshizato, Anal. Biochem. 302 (2002) 28–37.
[17] M. Tanaka, T. Hiragun, T. Tsutsui, Y. Yanase, H. Suzuki, M. Hide, Biosens. Bioelectron. 23 (2008) 1652–1658.
[18] R. Robelek, J. Wegener, Biosensors and Bioelectronics, Corrected Proof (2009) (In Press).
[19] M. Vala, S. Etheridge, J.A. Roach, J. Homola, Sens. Actuators B: Chem. 139 (2009) 59–63.
[20] C.-J. Huang, L. Mi, S. Jiang, Biomaterials 33 (2012) 3626–3631.
[21] C.J. Huang, J. Dostalek, W. Knoll, Biosens. Bioelectron. 26 (2010) 1425–1431.
[22] Y. Wang, A. Brunsen, U. Jonas, J. Dostalek, W. Knoll, Anal. Chem. 81 (2009) 9625–9632.
[23] M. Vala, J. Dostalek, J. Homola, Proc. SPIE 6585 (2009) 658521–658522.
[24] Y. Wang, W. Knoll, J. Dostalek, Anal. Chem. 84 (2012) 8345–8350.
[25] R. Slavík, J. Homola, Sens. Actuators B: Chem. 123 (2007) 10–12.
[26] R.V. Goreham, R.D. Short, K. Vasilev, J. Phys. Chem. C 115 (2011) 3429–3433.
[27] M.T. van Os, Surface modification by plasma polymerization film deposition tailoring of surface properties and biocompatibility, in: Department of Chemical Engineering, University of Twente, 2000, pp. 135.
[28] J. Dostálek, P. Adam, P. Kvasni?ka, O. Telezhnikova, J.í. Homola, Opt. Lett. 32 (2007) 2903–2905.
[29] C.J. Huang, J. Dostalek, W. Knoll, J. Vac. Soc. Technol. B 28 (2010) 66–72.
[30] K.S. Siow, L. Britcher, S. Kumar, H.J. Griesser, Plasma Process. Polym. 3 (2006) 392–418.
[31] B. Thierry, M. Jasieniak, L.C.P.M. de Smet, K. Vasilev, H.J. Griesser, Langmuir 24 (2008) 10187–10195.
[32] R.A. Innes, J.R. Sambles, J. Phys. F: Metal Phys. 17 (1987) 277.